Technical University of Denmark

DTU

The influence of roughness, angle, range, and transducer type on the echo signal from planar interfaces

Wilhjelm, Jens E.; Pedersen, Peter C.; Jacobsen, Søren Mehl

Link back to DTU Orbit

DTU Library
Technical Information Center of Denmark

The Influence of Roughness, Angle, Range, and Transducer Type on the Echo Signal from Planar Interfaces

Jens E. Wilhjelm, *Member, IEEE*, Peder C. Pedersen, *Senior Member, IEEE*, and Søren M. Jacobsen

Abstract—The received electrical echo signal from a pulse-echo system insonifying a planar interface was measured for varying degrees of rms roughness [0 to 0.29 mm (0 to 1.7 λ)], angles of incidence, θ, ($-7°$ to $7°$), and ranges to a planar or focused transducer. The effect of varying θ is quantified in terms of the energy of the received signal, $E(\theta)$, and the normalized spectrum of the received signal.

$E(\theta)$ is approximately Gaussian when using a planar transducer or a focused transducer with the reflecting interface located at or beyond the focal point. For focused transducers with the interface located closer than the geometrical point of focus, two maxima can sometimes be observed when varying the incident angle.

As is generally known, the width of $E(\theta)$ is strongly dependent on transducer type, e.g., for a smooth interface, the -3 dB width for a 25.4 mm diameter 5-MHz planar and focused transducer was approximately 0.5° and 4° (at the focal point), respectively.

$E(0°)$ as a function of surface roughness, R_q, was nearly linear on a decibel scale, with a slope of -109 dB / (R_q/λ) and -61 dB / (R_q/λ) for planar and focused transducers, respectively.

The characteristic nulls present in the normalized spectra of the echo signal at non-normal incidence tend to vanish with increasing R_q when using planar transducers. For focused transducers, the normalized spectra change from relatively flat to monotonically decreasing as R_q increases, and they exhibit reduced amplitude with increased incident angle.

I. Introduction

TISSUE characterization has been an active area of research for several decades. The progress has, however, been limited by the fact that the 1D electrical signal from the receiving transducer is the result of not only the 3D distribution of scatterers and the geometry and acoustic properties of interfaces, but also the field pattern and frequency response of the given transducer and constructive/destructive interference in the backscattered field at the surface of the receiving transducer.

As an example, the received electrical signal from a pulse-echo system insonifying a large planar interface de-

pends mainly on the surface characteristics and orientation of the interface and on transducer geometry. When the interface is smooth, the given measurement configuration can be simulated with computer models [1], [2] even when the interface is non-planar [3]. When a rough planar interface is considered, the modeling becomes stochastic in nature [4], and computer modeling tools are not yet available to readily predict the received electrical signal.

In conventional medical imaging with ultrasound, the angle between the beam and the various interfaces normally present in the image plane may vary throughout the image. Often just a single interface can be visualized at normal incidence. This creates an incident-angle dependent variation in image intensity [5], but this is not a serious problem as long as one does not need to derive acoustic properties (such as echogenicity or acoustic impedance) from the received signals. But any attempts of tissue characterization [or materials characterization in non-destructive evaluation (NDE)] need to be concerned with the influence of interface orientation, interface geometry (shape), and interface properties, such as roughness. The effects of these parameters are primarily manifested in the amplitude of the received electrical signal from the transducer, but also in the spectrum of this signal.

The scattering of acoustic and electromagnetic waves from rough interfaces has been an active area of research for decades in radar, sonar, and NDE applications and lately in diagnostic ultrasound. Specifically, ultrasound can be used to characterize surface parameters such as the rms roughness [6]–[14]. Operating in pulse-echo mode, one paper [9] reports on the influence of curvature of rough interfaces for the purpose of studying surface fibrillatory changes in osteoarthritic articular cartilage; another study [11] used time delay spectrometry with planar rough interfaces.

The goal of this paper is to attain a quantitative understanding of the received electrical signal from a pulse-echo system as a function of transducer geometry and the roughness properties of the interface. For this purpose, received signals were acquired for planar interfaces with varying degrees of rms roughness, angle of incidence, and range to the transducer, as depicted in Fig. 1.

The paper is structured as follows. Section II describes the manufacture and characterization of the rough interfaces, the experimental system, and the characterization of the single-element transducers. Sections III and IV explain the measurement procedure used to record the re-
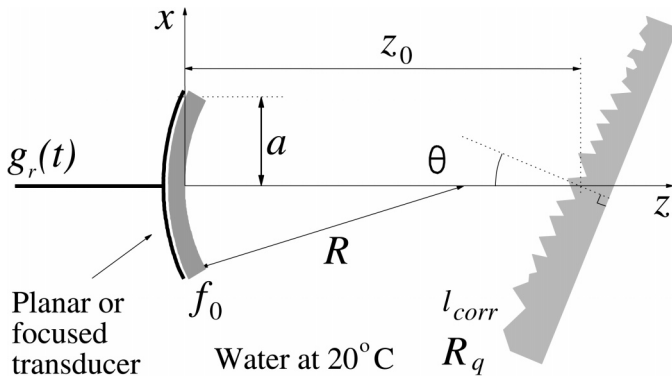
Fig. 1. Side view of the basic measurement set-up. A rough planar interface with rms roughness R_q and correlation length l_{corr} is rotated by angle θ with respect to normal incidence at a distance z_0 from a planar or focused transducer (radius of curvature, R) with radius a and center frequency f_0.

ceived signals and the signal processing used to extract the desired parameters from the received signals. Experimental results in the form of energy curves and frequency spectra as a function of angle, together with some derived parameters, are then provided in Section V. The results are finally discussed in Section VI.

II. Experimental System

A. Production and Characterization of Reflectors

Four rough and one smooth planar reflector phantoms were cast with a two-component, liquid urethane casting elastomer [Biresin®(type U1402), Sika Chemie GMBH, Stuttgart, Germany] using as molds four types of sandpaper with different degrees of roughness. This elastomer has acoustic properties very close to those of human tissues (speed of sound, $c = 1450$ m/s; density, $\rho = 1.06 \bullet 10^3$ kg/m^3 @ 20°C). This product has previously been used in phantoms, e.g., a realization of a so-called "dead zone array" [15] according to [16]. The molding took place in a vacuum to ensure that the phantom was an exact inverse copy of the sandpaper surface. Each phantom was supported by a 10- × 10-cm (inner dimensions) acrylic frame. It was verified that the reflector phantoms contained no voids or particles, so that a single acoustic interface between water and elastomer was obtained during measurements.

Measurement of several surface profiles directly on the sandpaper was carried out with a laser profilometer (type OTM3-10/144, UBM Messtechnik GMBH, Ettlingen, Germany), working in triangulation mode. Possible waviness, e.g., from bending of the sandpaper, in the profiles was removed by filtering the profiles with an 8th order highpass Butterworth filter with a cut-off frequency of 0.25 mm^{-1}. From the measured and filtered profile, $h(l)$, the rms [17]

TABLE I
OVERVIEW OF THE PROPERTIES OF THE REFLECTOR PHANTOMS USED IN THIS STUDY.

Sandpaper grid value	R_q (μm)	l_{corr} (μm)
Smooth	0	∞
p150	32	170
p100	89	155
p60	115	195
p40	155	290

roughness, R_q, was calculated as

$$R_q = \sqrt{\frac{1}{L} \int_0^L (h(l) - E_1\{h(l)\})^2 dl} \quad (1)$$

where L is the total length of the profile and $E_l\{h(l)\}$ is the mean of $h(l)$. The correlation length [18], l_{corr}, was calculated from the normalized autocorrelation function, $A_h(\tau)$, of $h(l)$. Specifically, in this work, l_{corr} is equal to the value of τ, where $A_h(\tau)$ has decreased to $1/e$ (or $\sim 37\%$).

Two profiles of length 20 mm and one of length 40 mm were recorded from each phantom, except the least rough phantom, for which only one 40-mm profile was recorded. To verify that the lengths of the profiles were adequate, R_q and l_{corr} were also calculated from profiles of one-half of the length; no noticeable changes in the estimated parameters were found. The results are given in Table I.

B. Ultrasound System

The electrical part of the measurement system is depicted in Fig. 2. The ultrasound system consisted of a pulser/receiver (type 5072PR, Panametrics, Inc., MA) connected to a submersible transducer (to be described in II-C). The amplified signal from the pulser/receiver was bandpass filtered to limit noise outside the useable frequency range of the particular transducer and digitized with a digital storage oscilloscope (DSO) (type 9450, LeCroy, Genève, Switzerland). The DSO was in turn connected via a general purpose interface bus (GPIB) interface to a Windows NT$^{\text{TM}}$-based control computer. By means of an RS232 interface, a 3D translation system (type 403020, Dyrbæk Technologies, Åbenrå, Denmark) was connected to this control computer as well.

Two specially developed software packages allowed direct control of the 3D translation system and direct setup of all relevant instrument parameters, including automatic adjustment of the vertical gain of the DSO, to ensure that the dynamic range of the eight-bit analog-to-digital converter was used optimally for each individual signal. To reduce random noise uncorrelated with the emitted signal, the received signal from the transducer was averaged 50 times in the DSO before transfer to the computer.

The experimental set-up is illustrated in Fig. 3. The transducer was mounted in the 3D translation system and adjusted such that its acoustic axis was parallel to the
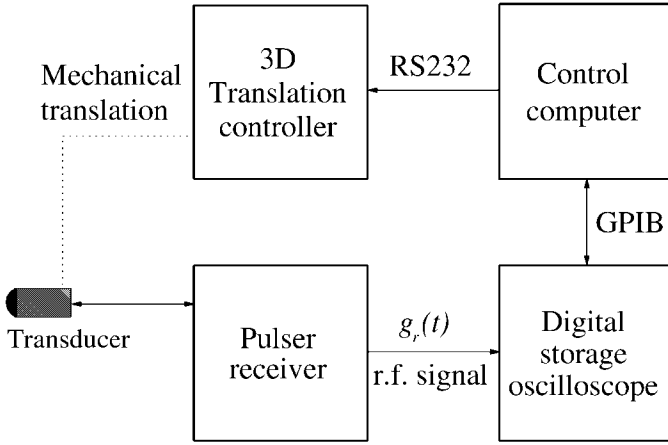
Fig. 2. Block diagram of the electrical part of the measurement system. A control computer is controlling the transducer position and reading the digitized signals from the digital storage oscilloscope.
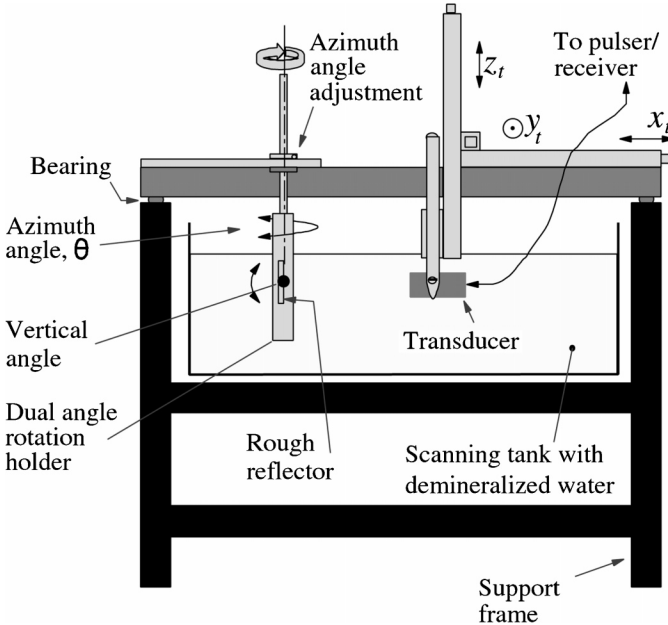

Fig. 3. The experimental system showing cross-sectional view of transducer and reflector phantom placed in dual-angle rotation holder, both submerged in demineralized degassed water.

x_t-axis. The holder in which the reflector phantom was mounted consisted of two frames that could be rotated independently of each other with the two axes of rotation normal to each other. Each reflector phantom was mounted such that the two axes of rotation were located in the plane of the interface between water and phantom. Measurements took place in degassed demineralized water at 20°C.

C. Transducer Characterization

As the results in this study depend highly on the transducer parameters, the seven different transducers utilized were all characterized based on a thorough field mapping

procedure. Specifically, each (focused or planar) transducer was mapped with a 0.4-mm hydrophone (Type MH-28-4, Force Institute, Brøndby, Denmark) with a useable bandwidth between 2 and 19.5 MHz (in which the sensitivity fluctuated less then 3 dB). From the hydrophone signals measured at parallel scan planes normal to the z-axis in Fig. 1, the acoustic axis was determined from the point of maximal intensity in each scan plane. The intensity along this axis was denoted $I(z)$. The value of z, where $I(z)$ was maximal, was identified and denoted z_{max}. The mean frequency, $\hat{f}_0$, and rms bandwidth [17], $B_{0,rms}$, of the hydrophone signal were both evaluated at this point in space. In addition, the rms lateral beamwidth, Δx_{rms}, was evaluated at this range as well. As the beam profile was approximately Gaussian, the -3 dB beamwidth can be estimated by multiplying Δx_{rms} by ~ 2.35 [17]. The values of these parameters are given in Table II.

The focused transducers were made with an acoustic lens. To find the radius of curvature, R, for an equivalently spherically focused crystal, an expression for the intensity on the acoustic axis for a spherically focused transducer [19]

$$I(z) = \left[\frac{R}{R-z} \sin \left(\frac{\pi a^2 \hat{f}_0 (R-z)}{2Rzc} \right) \right]^2 \qquad (2)$$

was used to iteratively estimate R. In (2), c is the speed of sound. Note that (2) was derived for the CW (continuous wave) case, and therefore gives approximate results when used for the pulsed wave (PW) case. The focusing strength at the estimated transducer center frequency, $\hat{f}_0$, was calculated as [20]

$$\gamma = \frac{a^2/\lambda^2}{R/\lambda} = \frac{a^2 \hat{f}_0}{cR}. \qquad (3)$$

As seen from Table II, the nominal center frequency (f_0) deviates from the measured mean frequency $\hat{f}_0$ for some transducers. A deviation was also observed when using the phantoms. The mean frequency of the spectrum used for normalization, i.e., the spectrum of the received signal at $\theta = 0°$ from a smooth interface, as will be described at the end of Section IV, was calculated from the experimental data at range $z_0 = 70$ mm for the planar transducers and $z_0 = R$ for the focused transducers. In general, the mean frequency determined this way was about 5% lower than the corresponding mean frequency based on the hydrophone data.

III. MEASUREMENT PROCEDURE

Prior to the measurements on the rough reflector phantoms, the transducer was adjusted so that its acoustic axis was parallel to the x_t-axis shown in Fig. 3. This was done by substituting the planar reflector with a 0.1-mm string (placed parallel with the z_t-axis) and recording the lateral beam profile at two different ranges. The alignment was

TABLE II

OVERVIEW OF THE TRANSDUCERS USED IN THIS WORK. ALL TRANSDUCERS WERE MADE BY PANAMETRICS (WALTHAM, MA). R AND γ WERE FOUND WITH (2) AND (3), RESPECTIVELY. Δx_{RMS} IS GIVEN APPROXIMATELY AT THE RANGE z_{max}.

		Specified parameters			Measured parameters				
ID in this paper	Model	f_0 (MHz)	a (mm)	R (mm)	$\hat{f}_0$ (MHz)	$B_{0,rms}$ (MHz)	z_{max} (mm)	Δx_{rms} (mm)	γ
P1	M306	2.25	6.35	∞	2.7	0.56	—	~3.5	—
P2	V304	2.25	12.7	∞	2.5	0.66	—	~7	—
P3	V307	5	12.7	∞	4.6	1.2	—	~7.5	—
F1[1]	M309	5	6.35	62	6	1.5	51.6	~1	2.6
F2[1]	V307	5	12.7	118	5.4	1.4	112	~1	4.9
F3[1]	V320	7.5	6.35	58.5	7.9	2.1	53.7	~0.75	3.6
F4[1]	V312	10	3.18	41.9	8.8	2.0	31.5	~1.1	1.4

[1] The four transducers, F1–F4, bore the inscription 'F = 2.5″ FPF', 'F = 120 mm FPF', 'F = 2″ PTF' and 'F = 60 MM OLF,' respectively.

successful when the centers of the two beam profiles, expressed in y_t-coordinates, were identical. This procedure was repeated with the string parallel with the y_t-axis. The plane of the frame in which the reflector phantoms were mounted was aligned to be normal to the acoustic axis of the transducer by measuring round trip travel times from the four corners of the frame.

Because air can be trapped at the surface of the rough reflector phantoms, these were degassed in a water bath in vacuum prior to use. Great care was taken to ensure that the surfaces were completely clean. When, for instance, a small mark with an overhead pen (China ink) was placed on the surface of the smooth phantom, the received signal magnitude doubled for the 7.5-MHz focused transducer as compared with a clean surface.

The angular span, $\pm\theta_{max}$, was chosen to be $\pm 7°$ because, at this angle, the energy of the received signal had changed sufficiently to allow visualization of the general behavior for most of the interfaces and transducers. In addition, over this angular range, the pressure reflection coefficient can be assumed constant (change is less than 1%). The increment, $\Delta\theta$, was varied over the angular recording range, so that the fine structure of the changes in the received signal as a function of angle could be recorded.

The measurements were performed with the reflectors placed at two distances to the planar transducers, $z_0 = 50$ and 70 mm, and at three distances for the focused transducers, $z_0 = 0.8R$, R, and $1.2R$. These specific ranges were also used in simulation studies for smooth interfaces [1], [2] and seemed to provide the best possible insight with the fewest possible measurements.

For each transducer, the surface of a given reflector phantom was divided into M equally spaced insonified regions, and one echo signal was recorded from the center of each region. For each angle and range, it was possible to record several independent received signals and from these obtain statistically stable estimates of the signal parameters. For any cell located off the azimuth (reflector) axis of rotation, this multi-cell recording technique required that the transducer was moved appropriately to keep a constant

distance to the reflector. After recording, this translation pattern was verified by checking the mean delay of the received signals. The total size of the scanned region on the phantom surface depended on the beamwidth but was always small enough so that echoes from the frames surrounding the phantom were negligible. The distance from the center of a cell to the edge of the phantom surface was at least 20 mm. M varied with transducer but was typically chosen to be around 20 to 30.

IV. SIGNAL PROCESSING

The first step of the signal processing involved visualization of the envelope of the received signal on a logarithmic scale (dB). This was done to inspect for possible temporal clipping of the received signals during recording and to identify the location and length of a rectangular window that was subsequently applied to exclude data points with pure noise. The duration of the received signal, i.e., when it was above the noise floor, varied with transducer, range, angle, and roughness; it was between 7 and 18 cycles at $\hat{f}_0$.

The received signal for the mth surface cell, at range z_0 from the reflector, rotated the angle θ, is denoted $g_r(t; m, \theta, z_0, R_q)$, where R_q is the rms roughness of the interface and $m \in [1; M]$.

The mean energy—over all M regions of the reflector surface—of the received signals was calculated as

$$E(\theta, z_0, R_q) = \frac{1}{M} \sum_{m=1}^{M} \int g_r^2(t; m, \theta, z_0, R_q)\, dt \tag{4}$$

where the integration covers the entire echo signal from the interface.

Subsample determination of the zero point for the θ-axis was next made by using the central part of $E(\theta, z_0, R_q = 0)$, where the energy had dropped less than 5 dB. $E(\theta, z_0, 0)$ as a function of θ had to be well behaved, e.g., Fig. 4 and Fig. 7(b), for planar and focused transducers,
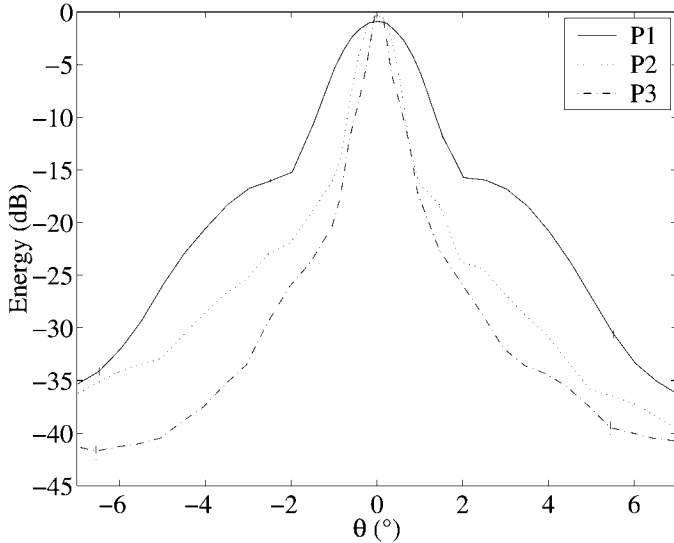
Fig. 4. Individually normalized curves of mean energy of received signals, $E_{N,dB}(\theta, z_0 = 70$ mm, $R_q = 0$ μm), from smooth planar interface for all planar transducers. (See Table II for parameters for the transducers P_1, P_2 and P_3.)

respectively; so, for focused transducers, $E(\theta, R, 0)$ was used.

The normalized mean amplitude spectrum is

$$G_{Norm}(f; \theta, z_0, R_q) = \frac{\dfrac{1}{M} \sum_{m=1}^{M} \left| \mathrm{FG}\{g_r(t; m, \theta, z_0, R_q)\} \right|}{\left| \mathrm{FT}\{g_r(t; 1, 0, z_0, 0)\} \right|} \quad (5)$$

where $\mathrm{FT}\{\bullet\}$ denotes Fourier transform. In (5), it is noted that the reference spectrum is equal to the spectrum of one particular received signal, $g_r(t; 1, 0^\circ, z_0, 0)$, recorded from the smooth interface at normal incidence. Ideally, the M signals from the smooth interface at zero degree should be identical. However, in the measurement situation, the surface of the smooth reflector phantom is not completely plane, so the angle of incidence is not exactly zero degree over the entire interface. (The deviation is estimated to be below 0.05°.) Thus, for planar transducers and focused transducers at the point of geometrical focus, the spectrum with the highest energy was identified and used for the normalization in (5). This spectrum was denoted $m = 1$.

V. RESULTS

A. Energy Versus Angle

$E(\theta, z_0, R_q)$ was measured for all combinations of transducers and phantoms; however, only a few representative plots of $E(\theta, z_0, R_q)$ will be provided. The behavior of the remaining energy versus angle functions will be described.

Because the p150 phantom was made with a mixture of Biresin, slightly different from the other phantoms, the reflection coefficient is slightly different. Thus, this phantom is not included in the plots of energy versus angle presented in this subsection.

All of the plots in this subsection are normalized so that 0 dB corresponds to the maximal energy recorded from a smooth interface with a given transducer, over all ranges and angles:

$$E_{N,dB}(\theta, z_0, R_q) = 10 \log_{10}\left(\frac{E(\theta, z_0, R_q)}{\max\limits_{\theta, z_0}\{E(\theta, z_0, 0)\}} \right). \quad (6)$$

Note that maximal energy is not necessarily obtained at 0°.

Fig. 4 shows $E_{N,dB}(\theta, z_0 = 70$ mm, $R_q = 0$ μm) for two different transducer frequencies and two different transducer radii. With the normalization done in (6), it should be noted that the maxima of the curves are slightly below 0 dB, because maximum energy was received at $z_0 = 50$ mm.

In Fig. 4 and all of the subsequent figures, vertical lines are added at a few locations on the plots to indicate the magnitude of the standard deviation (calculated over the M measurements) on $E_{N,dB}(\theta, z_0, R_q)$. The upper and lower point of each vertical line correspond to 10 $\log_{10}$ of the mean plus one standard deviation and the mean minus one standard deviation, respectively. Thus, the vertical lines are not located symmetrically around the mean. Note how these standard deviation lines for the smooth surface are only visible at high angles. When the interface becomes rough, the standard deviation increases dramatically.

Fig. 5 and 6 show $E_{N,dB}(\theta, z_0, R_q)$ for the two planar piston transducers with $a = 12.7$ mm. Because the transducers have different $\hat{f}_0$, the aperture—measured in λ at $\hat{f}_0$—differs for the two transducers. Notice the very small dependence on range, when comparing Fig. 6(a) with Fig. 6(b). This was the case for all planar transducers.

Fig. 7 shows $E_{N,dB}(\theta, z_0, R_q)$ for different ranges for the focused transducer F3. Notice in Fig. 7(a) how maximal energy is obtain at $\pm 2.4^\circ$, not 0°. The corresponding sets of curves for transducer F1 are very similar in shape to those of Fig. 7. Somewhat larger deviations from Fig. 7 were observed in the curves for transducers F2 and F4.

$E_{N,dB}(\theta, z_0, R_q)$ for planar and focused transducers can now be contrasted by comparing the curve for $R_q = 0.48\lambda$ in Fig. 6 with the curve for $R_q = 0.47\lambda$ in Fig. 7. A similar comparison can be done for the curves for $R_q = 0$.

For the flat transducers and for the focused transducers with the interface at range equal to the focal distance, R, or beyond, it can be seen that the energy as a function of angle has a nearly Gaussian shape with maximum at 0°. If the flat 5-MHz transducer, P3, was compared with the corresponding focused transducer, F2, (curves not presented), it was found that the -3 dB width of $E_{N,dB}(\theta, z_0, R_q = 0$ μm) was $\sim 0.5^\circ$ for the planar and $\sim 4^\circ$ for the focused transducer. The -3 dB width increases exponentially with rms roughness so that when $R_q \cong 155$ μm $\cong \lambda_0/2$, the
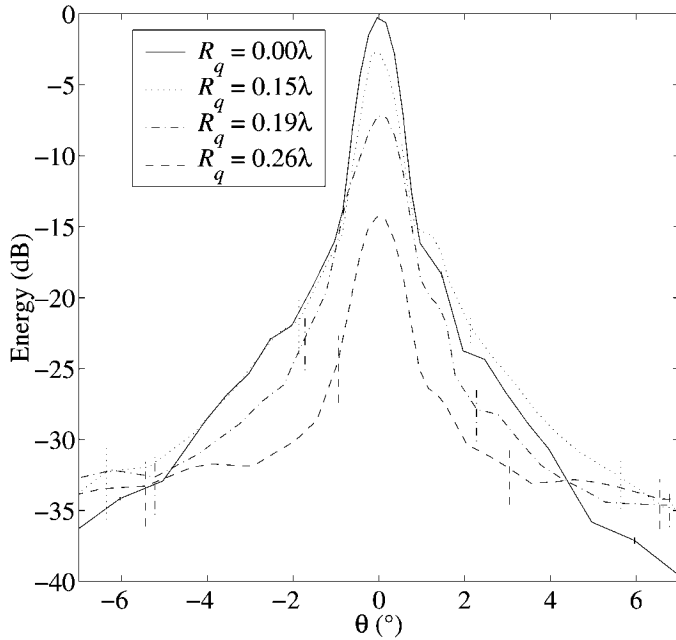
Fig. 5. Mean energy of received signals, $E_{N,dB}(\theta, z_0 = 70 \text{ mm}, R_q)$, from planar interfaces with various degrees of roughness for planar transducer P2 (a = 12.7 mm; $\hat{f}_0$ = 2.5 MHz).

energy is nearly constant inside the angular interval considered. The width of $E_{N,dB}(\theta, z_0, R_q)$ will be considered again in Fig. 9.

B. Derived Energy Measures

Various energy parameters were derived from the type of curves presented in Section V-A.

Fig. 8(a and b) depicts the mean energy at normal incidence, $E(\theta = 0°, z_0, R_q)$, as a function of surface roughness in wavelength for two planar and the four focused transducers, respectively. The energy levels for each transducer is normalized so that 0 dB corresponds to the energy received from the smooth surface. (This removes the variation in sensitivity of the individual transducers.) In both plots, all of the data points were used to estimate a "best-fit" linear regression line. Note that the data from phantom p150 are not included in this plot for the reason previously stated. Observe how the curves in Fig. 8(b) are rather independent on transducer type. Also, note that when $R_q/\lambda > 0.65$, the energy has dropped more than 40 dB and is consequently more influenced by noise.

Fig. 9 shows the angular width of $E(\theta, z_0, R_q)$, denoted $\Delta\theta_{0.9}$, which is defined by the levels where $E(\theta, z_0, R_q)$ has dropped to 90% of the maximal energy obtained at $0°$, as a function of rms roughness. As seen, in general, $\Delta\theta_{0.9}$ increases exponentially with rms roughness.

C. Spectra as a Function of Incident Angle

To obtain further insight into the underlying mechanism that governs $E(\theta, z_0, R_q)$, this subsection presents spectra of the received signal as a function of incident angle. In Fig. 10, four sets of spectra are shown, specifically
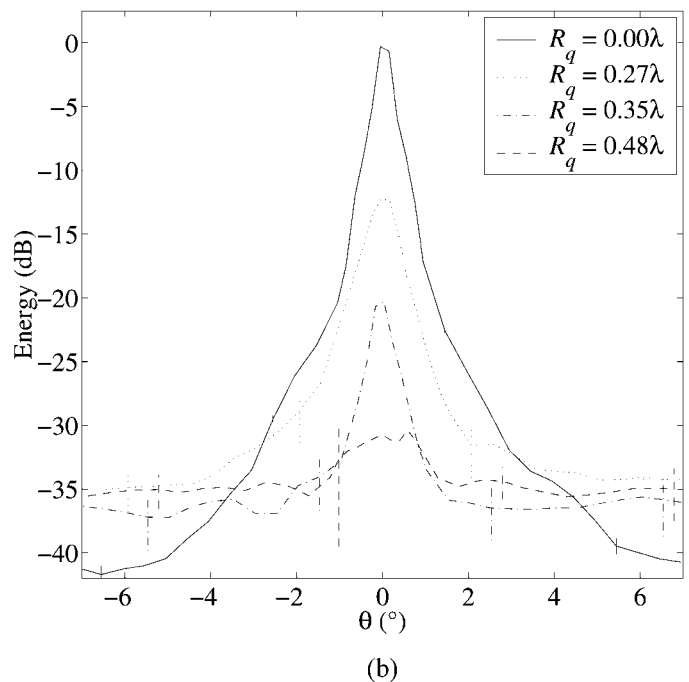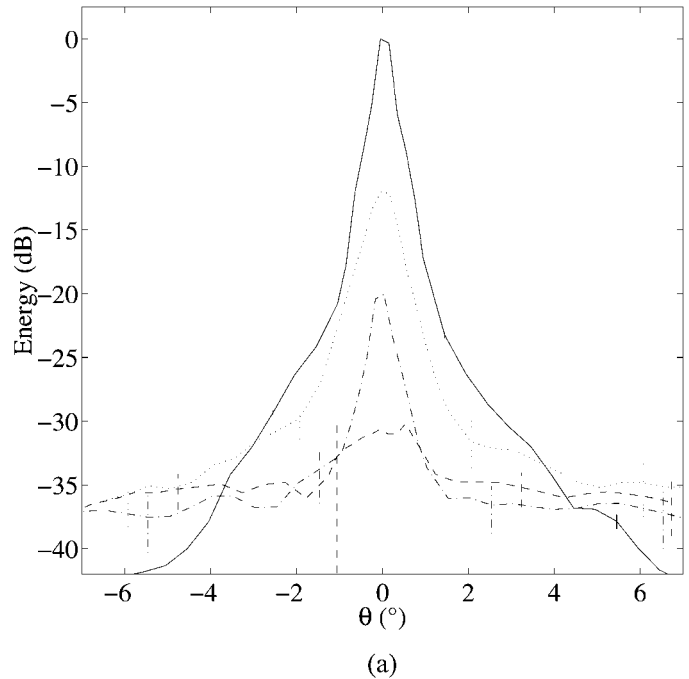

(a)

(b)

Fig. 6. Mean energy of received signals, $E_{N,dB}(\theta, z_0, R_q)$, from planar interfaces with various degrees of roughness for planar transducer P3 (a = 12.7 mm; $\hat{f}_0$ = 4.6 MHz) at ranges a) $z_0 = 50.5$ mm and b) $z_0 = 70.4$ mm.
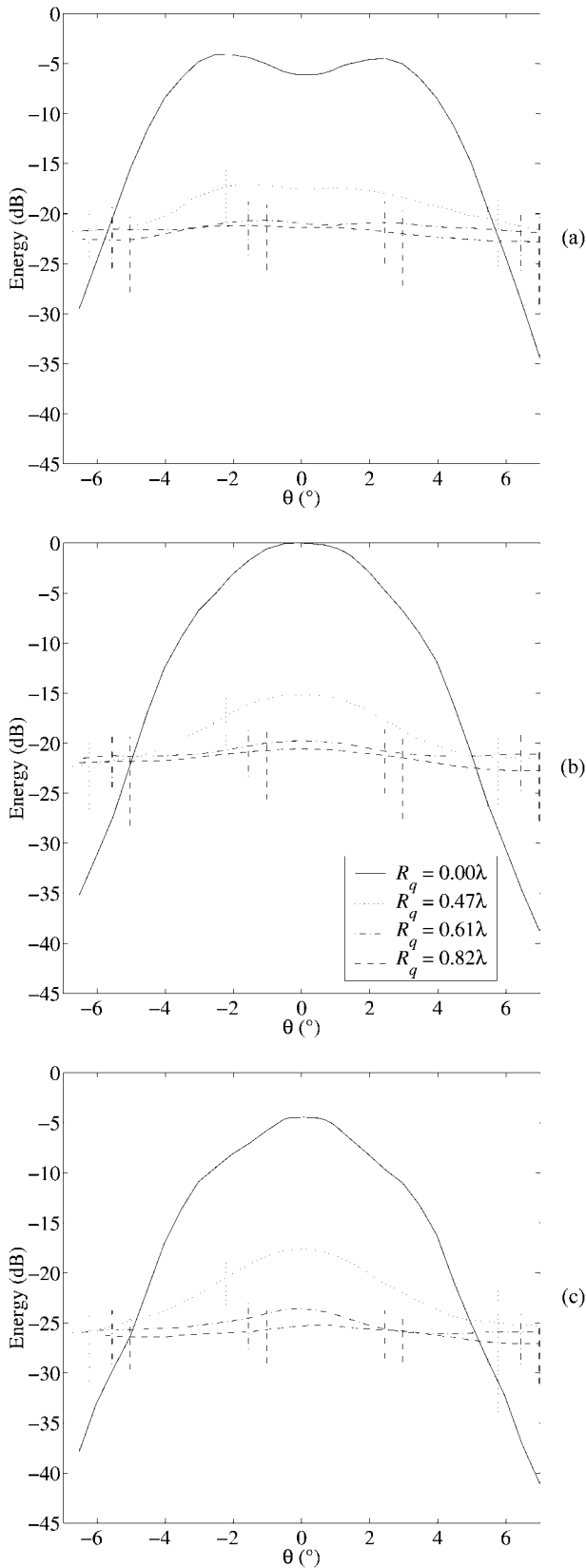
Fig. 7. Mean energy of received signals, $E_{N,dB}(\theta, z_0, R_q)$, for focused transducer F3 ($a = 6.35$ mm, $R = 58.5$ mm, $\hat{f}_0 = 7.9$ MHz) insonifying planar interfaces with various degrees of roughness placed at ranges a) $z_0 = 0.8R$, b) $z_0 = R$, and c) $z_0 = 1.2R$.
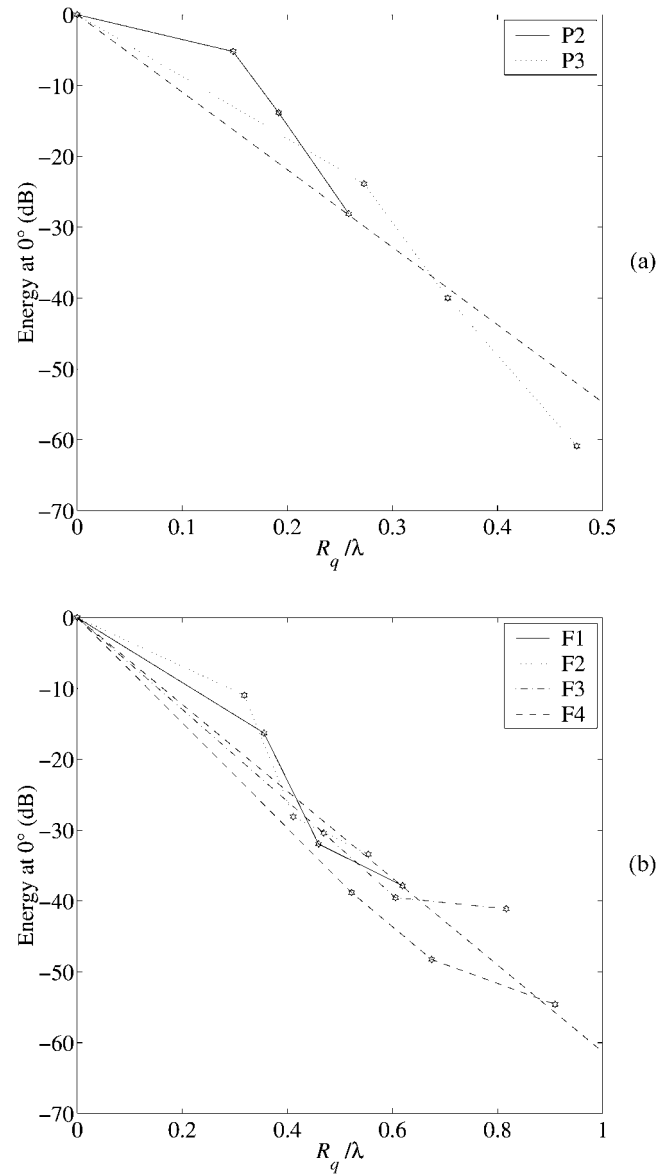

Fig. 8. Mean energy of received signal at $0°$ plotted as a function of rms roughness measured in wavelength for a) planar, $E_{N,dB}(\theta = 0°, z_0 = 50$ mm, $R_q)$, and b) focused, $E_{N,dB}(\theta = 0°, z_0 = R, R_q)$, transducers. The dashed line without markers shows the linear regression line. The slope is -109 dB / (R_q/λ) in (a) and -61 dB / (R_q/λ) in (b). In both plots, the correlation coefficient is 0.97. (See Table II for listing of transducer parameters.)

for a planar (P3) and a focused (F2) 5-MHz transducer, each insonifying either a smooth interface or an interface with an rms roughness of 32 μm. The interface was located at range $z_0 = 50$ mm from the flat transducer and at range $z_0 = R$ from the focused transducer. The wavelength at 5 MHz in 20°C pure water is approximately 300 μm. The spectra are shown in Fig. 10(a and c) for the smooth reflector phantom and in Fig. 10(b and d) for the p150 rough reflector phantom.
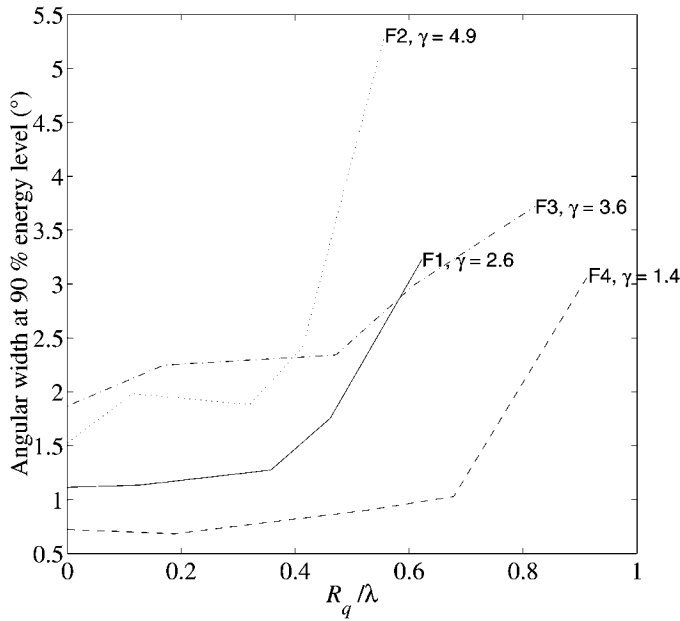
Fig. 9. The width in degree of $E(\theta, z_0 = R, R_q)$, where it has dropped to 90% of the maximal energy obtained at $0°$, $\Delta\theta_{0.9}$, for the four focused transducers in Table II. The indicated values of γ are used in Section VI.

VI. Discussion

A. General

The results presented in this paper might be relevant for future quantitative applications of ultrasound, such as attempts to relate measures of mean echogenicity or acoustic impedance with the material properties of the objects being scanned. Especially with respect to classification of atherosclerotic carotid plaque, such possibilities would be very attractive [21]–[25]. Another future application of the present results could be the verification of simulation models that can handle the measurement situation described here.

B. Energy

In general, $E(\theta)$ is approximately Gaussian when using a planar transducer or a focused transducer with the reflecting interface located at or beyond the focal point. Similar observations have been made by others. In more detail, for flat transducers, it was found that $E(\theta, z_0, R_q)$ is rather constant with z_0. Specifically, with the values of z_0 (50 and 70 mm) and the frequencies of the three planar transducers, $E(\theta, z_0, R_q)$ seems to be constant at least within $z_0 \in [84\lambda; 217\lambda]$. For focused transducers, $E(\theta, z_0, R_q)$ exhibits dramatic changes when $z_0 < R$; the dependence on range is much less when $z_0 \geq R$. This behavior corresponds to the behavior of the corresponding acoustic fields of the transducers, in the sense that $E(\theta, z_0, R_q)$ is smoother at ranges where the field fluctuates less.

When dealing with rough interfaces, several independent measurements of received signals are needed for a given set of experimental parameters to obtain statistically stable estimates. To give an impression of this, a few values of standard deviation have been added to the plots. In addition, the symmetry or lack of symmetry in the plots of $E(\theta, z_0, R_q)$ gives an indication of whether enough measurements were obtained from a given rough interface, albeit the reliability of this indicator decreases with the SNR. Thus, in Fig. 5, all curves for $E(\theta, z_0, R_q)$ are quite symmetrical; in Fig. 6, some of the curves begin to lack symmetry below ~ 30 dB.

Only a few of the papers that deal with measurements of rough surfaces have provided sufficiently detailed specification of the measurement parameters, so that comparisons with the present work are possible. Chiang *et al.* [9] measured curves similar to the ones presented in Section V-*A*, from sandpaper glued to acrylic rods to study the effect of finite surface curvature. They also used a smooth planar surface. For a planar transducer with $a = 11.8\lambda$, they found the width of $E(\theta)$ to be $\sim 4.7°$ at -10 dB. For transducer P1 in the present study, the corresponding width is $\sim 2.8°$. This discrepancy may be attributable to the larger transducer bandwidth used in the study by Chiang *et al.* [9], as well as to differences in transducer apodization and reflector material. For their focused transducer ($f_0 \sim 5$ MHz, $a = 3.2$ mm, $R \sim 16$ mm, $\gamma \sim 2.1$), the width was $\sim 12°$ at -10 dB. For transducer F1 (results not presented), the corresponding width was $6.7°$. If their smooth planar surface was substituted with a cylinder of diameter 19.1 mm and with an rms roughness of ~ 32 μm, the width was $16°$ at -10 dB. In our study, the corresponding width was $6.8°$. In both of the latter cases, the width measured in the present study is considerably smaller. This discrepancy is likely due to the fact that the radius of our transducer, a, was twice the radius of the one used in [9]. In addition, for the curved reflector, the curvature itself adds to the width of $E(\theta)$. Other reasons for the discrepancy can be differences in the signal processing and material of the reflector.

C. Derived Parameters

The general overall behavior of the results in Fig. 8 is as expected. However, the results also suggest that there exists a general, nearly linear, curve that describes the decrease in received energy at normal incidence with increase in rms roughness (at least for the range of transducer parameters used here). The observed slopes of $E(R_q)$ are a function of the characteristics of both the transmitting and the receiving transducer (identical in this work), and, given reciprocity, there is probably the same contribution from both. Not surprisingly, the slope of the corresponding regression line is larger for the planar transducer than for the focused transducer. For the receive part of the measurement situation, this can be physically explained by a larger phase cancellation effect on the receiving planar transducer than on the receiving focused transducer. The difference between the two slopes is also consistent with the difference between the slopes of the spectra at $0°$ in Fig. 10(b and d).
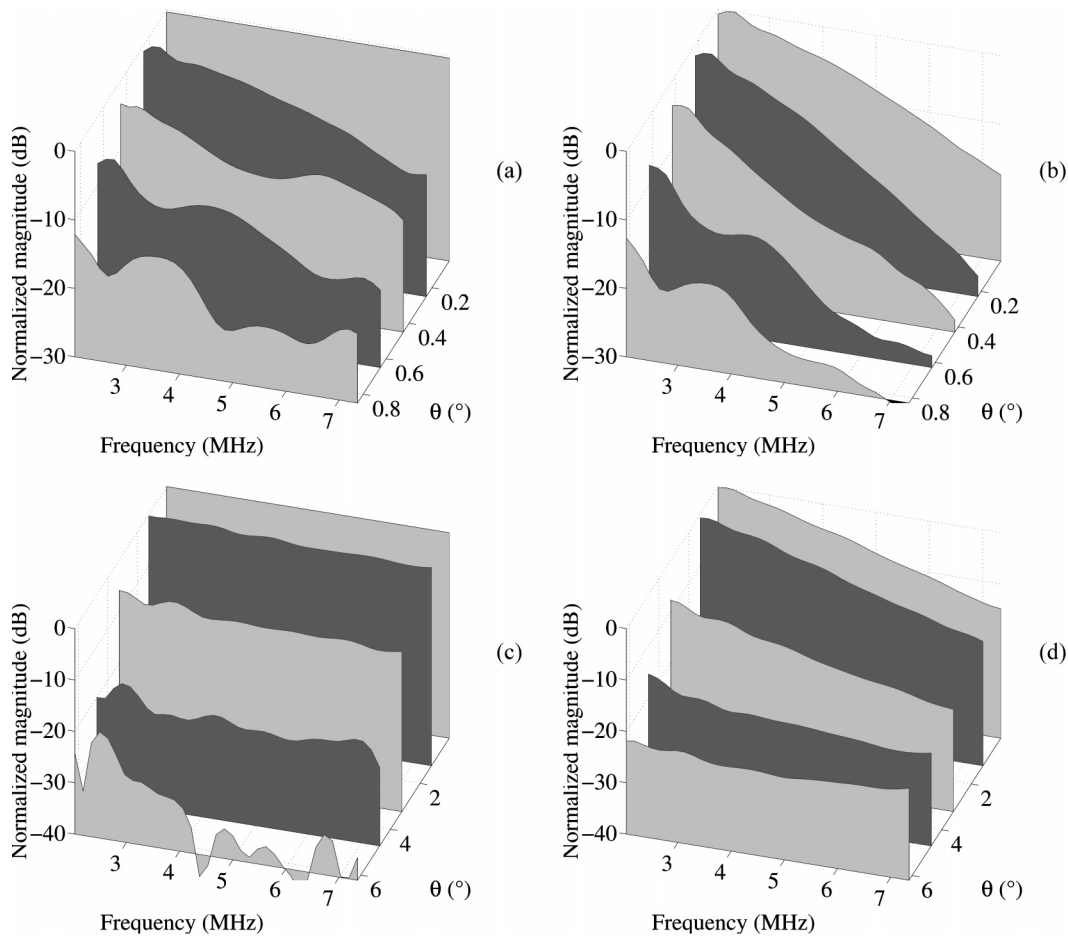
Fig. 10. Normalized spectra, $G_{Norm}(f; \theta, z_0, R_q)$, in decibels for planar transducer P3 a) and b) ($z_0 = 50$ mm) and focused transducer F2 c) and d) ($z_0 = R$). (a) and (c) are for a smooth interface ($M = 1$); (b) and (d) are for an interface with $R_q = 32\ \mu m = \lambda/10$ @ 5 MHz.

Fig. 8 can be compared with results obtained by Blessing and Eitzen [7] for the signal amplitude from rough surfaces at normal incidence. In their work, when R_q/λ increases from $\sim$0 to 0.15, the amplitude dropped from $\sim$0 to $\sim$13 dB. This is in fairly good agreement with Fig. 8(a).

The results in Fig. 9 indicate that the width, $\Delta\theta_{0.9}$, of $E(\theta, z_0, R_q)$ increases exponentially with rms roughness. However, if the degree of focusing (γ) is considered as a parameter in Fig. 9, it can be observed that there also seems to be an increase with γ. Fig. 9 also suggests that the surfaces appear quite smooth up to $R_q/\lambda \sim 0.4$.

Some small inconsistencies are connected with the latter observation though. For small R_q, the curve for $\gamma = 3.6$ lies slightly above the curve for $\gamma = 4.9$. For $R_q \sim 0.8\lambda$, the value for the curve $\gamma = 3.6$ is lower than expected, but, for this R_q (p40 phantom), the estimate of $E(\theta, z_0, R_q)$ is also the poorest. The lack of consistency for $R_q = 0$ (where the SNR is high) indicates that either the transducer does not behave in a similar manner (maybe the apodization for $\gamma = 3.6$ is different from the remaining transducers) or there are more factors influencing the results, such as the radius of the transducer, a, or the frequency content of the emitted signal. It can also be that the assumption of an equivalent radius of curvature is "wrong." Yet another possibility is the influence of the $\lambda/4$ matching layer. However, a possible relation between $\Delta\theta_{0.9}(R_q/\lambda)$ and γ (or another transducer parameter) should be studied further. However, such studies are very demanding both as simulation studies and as experimental work.

Information about the angular sensitivity, as depicted by plots of the type in Fig. 9, can have potential application in evaluation of scanning acoustic microscopes, where the very high acoustic frequency makes the alignment very critical, especially when reflection coefficients are to be measured. From the results in this paper, experiments involving planar transducers [26], [27] need to be more carefully aligned than those involving focused transducers [28], [29]. However, from the results presented in this study, it is not possible to directly evaluate the above mentioned investigations, because the transducer parameters differ too much and the surface roughness is unknown.

D. Spectra

1. Planar Transducers: For the smooth interface, the normalized spectrum has a negative slope with increasing angle of incidence and exhibits an increasing number of nulls with increased incident angle, as also predicted from numerical modeling [1]. There are some minor dif-

ferences between the experimental results and the simulation results which are probably due to the transducer's non-ideal behavior. Increasing the rms roughness made the null locations less distinct as seen in Fig. 10(b). Nevertheless, the overall picture remains the same, indicating that at $R_q \leq \lambda/10$ and angles below ~1°, the echo signal is still governed mainly by specular reflection. These observations suggest that the reduction in received signal energy with increased incident angle for a smooth interface is attributable to coherent phase cancellation over the surface of the transducer. As the rms roughness of the reflector becomes larger, the reflected pressure field becomes more incoherent, giving a reduction in the amount of phase cancellation that will occur when the angle of incidence is increased.

2. Focused Transducers: For the smooth interface, the angle-dependence was reduced compared to the planar transducer, and the null pattern was much less distinct (Fig. 10(c)). At $\theta \cong 6°$, strong phase cancellation (the nulls) seems to dominate together with an overall attenuation of ~30 dB (Snell's law). For the rough interface at lower angles (Fig. 10(d)), as the frequency increases, the specular reflection seems to be slowly substituted with weaker scattering, yielding the negative slope of the frequency spectra in Fig. 10(d). At $\theta \cong 6°$, a comparison of Fig. 10(c and d), indicates that the scattering component takes over and thus maintains a nearly constant spectrum.

The above findings suggest that for smooth interfaces, both phase cancellation of the received field on the transducer surface and Snell's law, are responsible for the drop in $E(\theta, z_0, R_q)$ with angle. When the interface becomes rough these two effects are then accompanied by (and gradually substituted with) Rayleigh scattering.

VII. Conclusions

Received electrical signals have been recorded from planar interfaces with varying degrees of roughness at different range for insonification angles from −7° to 7°. In general, the energy of the received signal decreases with increasing insonification angle due to phase cancellation of the received acoustic field at the transducer surface and Snell's law. The echo signal from planar transducers is more sensitive to changes in insonification angle (around 0°) than focused transducers. The width of the energy curves—describing the energy of the received signal as a function of angle—has been plotted against rms roughness for transducers with various focusing strength. This plot showed a tendency towards wider energy curves for higher focusing strength. The energy of the echo signal recorded at normal incidence also decreases with increasing rms roughness. This effect is much more pronounced for planar transducers than focused transducers.

The normalized spectra of the received echo signal for planar transducers insonifying a smooth interface showed a drop in magnitude with frequency and exhibited characteristic nulls whose spectral spacing decreases with increasing incident angle. For focused transducers with the reflector placed at the focal point, the normalized spectrum is relatively flat, with a level that decreases with angle.

References

[1] D. P. Orofino and P. C. Pedersen, "Angle-dependent spectral distortion for an infinite planar fluid-fluid interface," *J. Acoust. Soc. Amer.*, vol. 92, no. 5, pp. 2883–2899, 1992.

[2] P. C. Pedersen and D. P. Orofino, "Modeling of received ultrasound signals from finite planar targets," *IEEE Trans. Ultrason., Ferroelect., Freq. Contr.*, vol. 43, no. 2, pp. 303–311, 1996.

[3] S. K. Jespersen, P. C. Pedersen, and J. E. Wilhjelm, "The diffraction response interpolation method," *IEEE Trans. Ultrason., Ferroelect., Freq. Contr.*, vol. 45, pp. 1461–1475, 1998.

[4] B. J. Dean and P. C. Pedersen, "Angular spectrum based formulation of rough surface scattering with applications to surface characterization," in *Proc. 1996 IEEE Int. Ultrason. Symp.*, pp. 693–696.

[5] S. K. Jespersen, J. E. Wilhjelm, and H. Sillesen, "Multi-angle compound imaging," *Ultrason. Imaging*, vol. 20, pp. 81–102, 1998.

[6] M. D. Billy, F. Cohen-Ténoudji, A. Jungman, and G. J. Quentin, "The possibility of assigning a signature to rough surfaces using ultrasonic backscattering diagrams," *IEEE Trans. Sonics Ultrason.*, vol. 23, no. 5, pp. 356–363, 1976.

[7] G. V. Blessing and D. G. Eitzen, "Surface roughness sensed by ultrasound," *Surface Topography*, vol. 1, pp. 253–267, 1988.

[8] O. Bozma and R. Kuc, "Characterizing pulses reflected from rough surfaces using ultrasound," *J. Acoust. Soc. Amer.*, vol. 89, pp. 2519–2531, 1991.

[9] E. H. Chiang, R. S. Adler, C. R. Meyer, J. M. Rubin, D. K. Dedrick, and T. J. Laing, "Quantitative assessment of surface roughness using backscattered ultrasound: The effects of finite surface curvature," *Ultrasound Med. Biol.*, vol. 20, no. 2, pp. 123–135, 1994.

[10] S. J. Oh, Y. C. Shin, and E. S. Furgason, "Surface roughness evaluation via ultrasonic scanning," *IEEE Trans. Ultrason., Ferroelect., Freq. Contr.*, vol. 41, no. 6, pp. 863–871, 1994.

[11] P. C. Pedersen and A. Grebe, "Application of time delay spectrometry for rough surface characterization," *Ultrasonics*, vol. xx, no. x, pp. xx–xx, 1999.

[12] G. Quentin, M. D. Billy, F. C. Ténoudji, J. Doucet, and A. Jungman, "Experimental results on the scattering of ultrasound by randomly or periodically rough surfaces in the frequency range 2 to 25 MHz," in *Proc. IEEE Ultrason. Symp.*, 1975, pp. 102–106.

[13] P. D. Thorne and N. G. Pace, "Acoustic studies of broadband scattering from a model rough surface," *J. Acoust. Soc. Amer.*, vol. 75, pp. 133–144, 1984.

[14] P. J. Welton, H. G. Frey, and P. Moore, "Experimental measurements of the scattering of acoustic waves by rough surfaces," *J. Acoust. Soc. Amer.*, vol. 52, no. 5, pt. 2, pp. 1553–1563, 1972.

[15] Standard phantom 490. Danish Phantom Design: Gondolvej 25, 4040 Jyllinge, Denmark (www.fantom.suite.dk).

[16] "Ultasonics—Real-time pulse-echo systems—Test procedures to determine performance specifications," CEI, Genève, Suisse, IEC document 1390, 1996, fig. A.3.

[17] J. E. Wilhjelm, "Bandwidth expressions of Gaussian weighted chirp," *Elec. Lett.*, pp. 2161–2162, 1993.

[18] D. J. Whitehouse, *Handbook of Surface Metrology.* Institute of Physics Publishing, 1994.

[19] G. Kossoff, "Analysis of focusing action of spherically curved transducers," *Ultrasound Med. Biol.*, vol. 5, pp. 359–365, 1979.

[20] C. R. Hill, *Physical Principles of Medical Ultrasonics*. Chichester, England: Ellis Horwood Limited, 1998.

[21] N. M. El-Barghouty, T. Levine, S. Ladva, A. Flanagan, and A. Nicolaides, "Histological verification of computerised carotid plaque characterisation," *Eur. J. Vasc. Endovasc. Surg.*, vol. 11, pp. 414–416, 1996.

[22] European Carotid Plaque Study Group (ECPSG), "Carotid artery plaque composition—Relationship to clinical presentation and ultrasound B-mode imaging," *Eur. J. Vasc. Endovasc. Surg.*, vol. 10, pp. 23–30, 1995.

[23] T. M. Feeley, E. J. Leen, M.-P. Colgan, D. J. Moore, D. O. Hourihane, and G. D. Shanik, "Histologic characteristics of carotid artery plaque," *J. Vasc. Surg.*, vol. 13, no. 5, pp. 719–724, 1991.

[24] T. F. O'Donnell, L. Erdoes, W. C. Mackey, J. McCullough, A. Shepard, P. Heggerick, J. Isner, and A. D. Callow, "Correlation of B-mode ultrasound imaging and arteriography with pathologic findings at carotid endarterectomy," *Arch. Surg.*, vol. 120, pp. 443–449, 1985.

[25] J. E. Wilhjelm, M.-L.M. Grønholdt, B. Wiebe, S. K. Jespersen, L. K. Hansen, and H. Sillesen, "Quantitative analysis of ultrasound B-mode images of carotid atherosclerotic plaque: Correlation with visual classification and histological examination," *IEEE Trans. Med. Imaging*, vol. 17, no. 6, pp. 910–922, 1998.

[26] J. Kushibiki, N. Akashi, T. Sannomiya, N. Chubachi, and F. Dunn, "VHF/UHF range bioultrasonic spectroscopy system and method," *IEEE Trans. Ultrason., Ferroelect., Freq. Contr.*, vol. 42, no. 6, pp. 1028–1039, 1995.

[27] J. Kushibiki, M. Ishibashi, N. Akashi, T. Sannomiya, and N. Chubachi, "Transmission line method for the measurement of the acoustic nonlinearity parameter in biological liquids at very high frequencies," *J. Acoust. Soc. Amer.*, vol. 102, no. 5, pp. 3038–3044, 1997.

[28] N. Chubachi, J. Kushibiki, T. Sannomiya, and N. Akashi, "Scanning acoustic microscope for quantitative characterization of biological tissues," *Acoust. Imaging*, vol. 16, pp. 277–285, 1988.

[29] M. C. Zimmerman, A. Prabhakar, B. V. Chokshi, N. Budhwani, and H. Berndt, "The acoustic properties of normal and imbedded bovine bone as measured by acoustic microscopy," *J. Biomed. Mater. Res.*, vol. 28, pp. 931–938, 1994.

Peder C. Pedersen (S'74-M'76-SM'87) was born in Kalundborg, Denmark. He received the B.S. degree in electrical engineering from Aalborg Engineering College, Aalborg, Denmark, in 1971, and the M.E. and Ph.D. degrees in bioengineering from the University of Utah, Salt Lake City, in 1974 and 1976, respectively. In October 1987 he joined the faculty at Worcester Polytechnic Institute in Worcester, MA. He is a professor in the Electrical and Computer Engineering Department. Previously, he was an Associate Professor in the Department of Electrical and Computer Engineering at Drexel University, Philadelphia, and a core faculty member of Drexel's Biomedical Engineering and Science Institute.

His research areas include modeling of acoustic systems; characterization of rough surfaces based on scattered signals; Doppler flow systems utilizing FM excitation; and ultrasound-based measurement of mechanical properties of blood vessels. Specific applications include characterization of atherosclerotic plaque and ultrasound-based assessment of osteoporosis.

Dr. Pedersen is a member of Eta Kappa Nu, Sigma Xi, the Acoustical Society of America, and a senior member of the IEEE. He is an Advisory Board member of CRC Critical Reviews in Biomedical Engineering and a Registered Professional Engineer in the Commonwealth of Pennsylvania.

Søren Mehl Jacobsen was born 1971 in Aalborg, Denmark. In 1997 he received the M. Sc. degree in Electrical Engineering from the Technical University of Denmark. His master thesis dealt with surface roughness measurement using ultrasound. From 1998 to 2000 he has been employed as R&D engineer in the field of underwater acoustics at Reson A/S, Slangerup, Denmark. He is currently working with embedded software design at Logos Smart Card A/S, Lyngby, Denmark.

Jens E. Wilhjelm (S'86–M'86–S'88–M'91) was born in Copenhagen, Denmark. He received the M.Sc. degree in electrical engineering from the Technical University of Denmark in 1986 and the Ph.D. degree in biomedical engineering in 1991 from Worcester Polytechnic Institute, Worcester, MA. From 1986 to 1988 he worked with blood flow measurements in the ultrasonic laboratory at Brüel & Kjær A/S, Nærum, Denmark. In 1991, he came to the Electronics Institute, Technical University of Denmark where he held various fellowship positions until he became an associate professor in 1997 at the Department of Information Technology (now Ørsted.DTU).

His current research interests in medical diagnostic ultrasound includes technical and medical aspects within classification of atherosclerotic plaque, signal processing, and Doppler based blood flow measurements.

Dr. Wilhjelm is a member of the IEEE.